POLITECNICO DI TORINO
Repository ISTITUZIONALE

# Co-Casting of Al and Al-Foams

*Original*
Co-Casting of Al and Al-Foams / Ferraris, Sara; Santostefano, Antonio; DE MARCO, Frediano; Campagnoli, Elena; Matteis, Paolo; Barbato, Antonio; Molina, Roberto; Ubertalli, Graziano. - In: ADVANCED ENGINEERING MATERIALS. - ISSN 1527-2648. - ELETTRONICO. - (2022), p. 2200116. [10.1002/adem.202200116]

*Availability:*
This version is available at: 11583/2960351 since: 2022-04-01T11:02:38Z

*Publisher:*
Wiley

*Published*
DOI:10.1002/adem.202200116

*Terms of use:*

This article is made available under terms and conditions as specified in the corresponding bibliographic description in the repository

*Publisher copyright*

(Article begins on next page)

17 December 2025

ADVANCED ENGINEERING MATERIALS
www.aem-journal.com

# Co-Casting of Al and Al-Foams

*Sara Ferraris,* Antonio Santostefano, Frediano De Marco, Elena Campagnoli, Paolo Matteis, Antonio Barbato, Roberto Molina, and Graziano Ubertalli*

**The use of metal foams as permanent cores in casting products is a promising strategy. It aims to improve the properties of the cast components by adding certain foam features (e.g., lightweight, high specific stiffness, impact energy/vibration absorption ability, and good acoustic insulation properties). The use of permanent cores eliminates the steps of removal, treatment, and compulsory recycling for the traditional temporary sand cores. Herein, aluminum metals foams, in the form of bars with a dense continuous outer skin, are inserted in the die of a gravity casting experiment with an Al–Si–Cu–Mg alloy (EN AB.46400). Foams and cast objects are characterized by means of optical emission spectrometry (OES), optical microscopy (OM), scanning electron microscope equipped with energy dispersive spectroscopy (SEM-EDS), image analysis, and computed tomography (CT).**

## 1. Introduction

Metal foams are porous metallic materials characterized by lightweight, impact and vibration absorption ability, acoustic and thermal insulation properties.[1,2] These features make them extremely interesting for automotive and aerospace applications, where weight reduction and energy absorption are crucial properties. However, aluminum foams alone often do not match the requirements of the final products and have to be more effectively coupled with dense metal in the form of sandwiches or hollow structures with a foam core.[3,4]

The use of metal foams as permanent cores in cast products represents an interesting strategy to combine the properties of the foam (lightweight, impact absorption ability, thermal and acoustic insulation) with those of dense metal. Moreover, this solution allows the production of hollow structures by casting routes and eliminates the need to remove and recycle traditional temporary sand cores.

Despite being a promising industrial interest for this topic, this technology is still poorly explored in the scientific literature as well as in industrial applications, as evidenced by recent reviews.[5,6] In particular, various aluminum metal foams (e.g., Alporas, Formgrip, or Alulight type, with or without an external continuous skin) have been used as cores in gravity casting experiments[7,8] or high pressure die casting experiments[9,10]; however, most of them report few details on samples preparation and characterization. Nevertheless, all reported research state that the presence of external skin is fundamental to avoid the infiltration of the molten metal in the foam, which instead happens in the case of foam cores without surface skin. In some cases,[7,9] no bonding between the dense Al shell and the foam core was observed and this was explained considering the presence of stable aluminum oxides on the foam surface. In other cases,[8,10] a good core–shell bonding was obtained and it was attributed to a partial surface melting of the foam skin during the pouring process. In these cases, surface chemical composition (presence of oxides) was not discussed in the reported papers. To improve core–shell bonding, foam sandblasting,[7] or Zn-based coatings[9] have been proposed as possible strategies. Moreover, the paucity of literature reports on the improvement of core–shell bonding for aluminum foams in casting technologies means that some suggestions for the development of successful strategies of surface modifications and coatings can be found in other works which relate to the joining of aluminum alloys and foams,[11–15] such as cleaning, grinding,

S. Ferraris, A. Santostefano, P. Matteis, G. Ubertalli
Department of Applied Science and Technology
Politecnico di Torino
Corso Duca degli Abruzzi 24, 10129 Torino, Italy
E-mail: sara.ferraris@polito.it

F. De Marco
Advanced Joining Technologies at Politecnico di Torino Inter-Dipartimental Laboratory (J-TECH@POLITO
Corso Duca degli Abruzzi 24, 10129 Torino, Italy

E. Campagnoli
Department of Energy
Politecnico di Torino
Corso Duca degli Abruzzi 24, 10129 Torino, Italy

A. Barbato
R&D
DACA_I Powertrains Engineering Srl
Via Giuseppe Giacosa 38, 10125 Torino, Italy

R. Molina
Production
TEKSID ALUMINUM SRL
Via Umberto II, Carmagnola (TO), Italy

The ORCID identification number(s) for the author(s) of this article can be found under https://doi.org/10.1002/adem.202200116.

© 2022 The Authors. Advanced Engineering Materials published by Wiley-VCH GmbH. This is an open access article under the terms of the Creative Commons Attribution-NonCommercial-NoDerivs License, which permits use and distribution in any medium, provided the original work is properly cited, the use is non-commercial and no modifications or adaptations are made.

**DOI: 10.1002/adem.202200116**

acid or plasma etching in order remove the oxide layer and to reactivate the exposed metal surface.

Integral foam molding technique (IFM)[16] has also been proposed as single-step technology to obtain a dense shell around a foam core.

Two of the possible applications which have been explored are a crash absorber and an engine mount with a foam core, surrounded by a cast shell[3]; these examples, along with several patents on the use of foam cores in casting,[17–20] confirm the industrial interest for this co-casting technology.

The difficulties in the practical application of the co-casting strategy may also be associated with the inhomogeneity of the metal foams, which depends on the most diffused technological processes, which are mainly based on pore formation due to gas generation.[5] These production methods can lead to difficulties in controlling the process, as well as to high costs.[4]

In the present research work, aluminum foams with a dense continuous external skin were used as cores in gravity casting experiments. The foams were characterized by means of optical emission spectrometry (OES), optical microscopy (OM), scanning electron microscope equipped with energy dispersive spectroscopy (SEM-EDS), computed tomography (CT), thermal conductivity measurements, and image analysis to determine their chemical composition, thermal conductivity, porosity, skin thickness, microstructure, surface morphology, and composition. For the foam surface skin, a low-cost surface treatment for the improvement of core–shell bonding was carried out, tested, and characterized, both before and after co-cast component production. The cast objects were analyzed with some of the previously reported techniques to investigate the chemical composition, the eventual foam infiltration after casting, the possible bonding, and the microstructure of the cast metal. Moreover, during the experiments, the temperatures of the foam inserts, of the molten metal, and of the die were recorded to better investigate the thermal behavior of the foams during the casting process.

## 2. Experimental Section

### 2.1. Al Foams

Aluminum metal foams (AlMgSi1 alloy with a limited amount of $TiH_2$ as a foaming agent) with a dense outer skin, produced by the powder metallurgy technique were purchased from Havel Metal Foams GmbH in the form of rectangular bars (transversal section: 22 × 12.7 or 12 mm) cut at a length of 122 mm.

Samples of three different nominal densities (1.0, 1.3, and 1.5 g cm$^{-3}$, defined as Foam 1, Foam 2, and Foam 3 respectively) were used for the experiments (**Figure 1**).

Both the extremities of the foam inserts in position II were milled to ensure for one side, after mounting, the direct thermal contact with the mobile part of the die, as shown in **Figure 2**b.

### 2.2. Casting Experiments

Gravity casting experiments were performed in the present research.

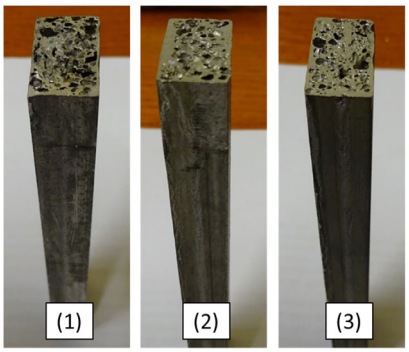


**Figure 1.** Images of foam inserts: 1) Foam 1, 2) Foam 2, and 3) Foam 3.

A scheme of the die, with the indication of the insertion zone of foams cores—inserts, is reported in Figure 2a. The specific design of the die foresees two steps of different thickness (step 1—6 mm and step 2—11 mm) without foam inserts and two steps with foam inserts (step 3 and step 4) and nominal thickness of the dense metal around the foam analogous to that of the dense steps (6 mm for step 3 and 11 mm for step 4). One casting experiment for each type of foam as the insert was performed.

Three thermocouples were introduced (one for each foam insert and one in molten aluminum) to monitor the temperature of the different elements during the experiments (Figure 1a). Moreover, a fourth thermocouple was inserted in the mobile side of the die to record the die temperature too.

The Al–Si–Cu–Mg alloy (EN AB.46400) was used for casting, maintaining the liquid at 720 °C, and poured into the die, where the foams inserts were previously positioned (Figure 2b). The foam introduced in position (I) (Figure 2a), corresponding to step 4 in the final cast object, has a thickness of 12.7 mm and is mounted to be completely surrounded by the molten metal during casting. The foam introduced in position (II) (Figure 2a), corresponds to step 3 in the final cast object, has a thickness of 12 mm, and is mounted to maintain a face free from the molten metal and in direct contact with the mold wall. These arrangements of the two cores were defined to analyze the cooling rate influence during the solidification of the poured metal in contact with the foamed core.

In the first set of experiments, the as-received Al-foams bars were inserted in the die for gravity casting (Figure 2b), without specific surface treatments or heating. In the second set of experiments, the foam surfaces were grinded with abrasive paper (SiC abrasive—320 grit) and nitric acid (12%) etched, using the same optimized method adopted from the authors in the brazing of aluminum foams to aluminum sheets.[15] In the second experiment, the foam insert with thermocouple was in position I, and the thermocouple for measuring the liquid temperature was in position II (Figure 2a), instead of in the melt pool as indicated in Figure 2a for the first experiment. No foam insert was introduced in position II in this second test.

It must be pointed out that the foam core, placed in position (I)—Figure 2, has a small contact area with the die walls (which are about at 250 °C) only at both ends; therefore, when the mobile part of the mold is closed and before pouring, it does not completely touch the moving part and heats more slowly than


© 2022 The Authors. Advanced Engineering Materials published by Wiley-VCH GmbH

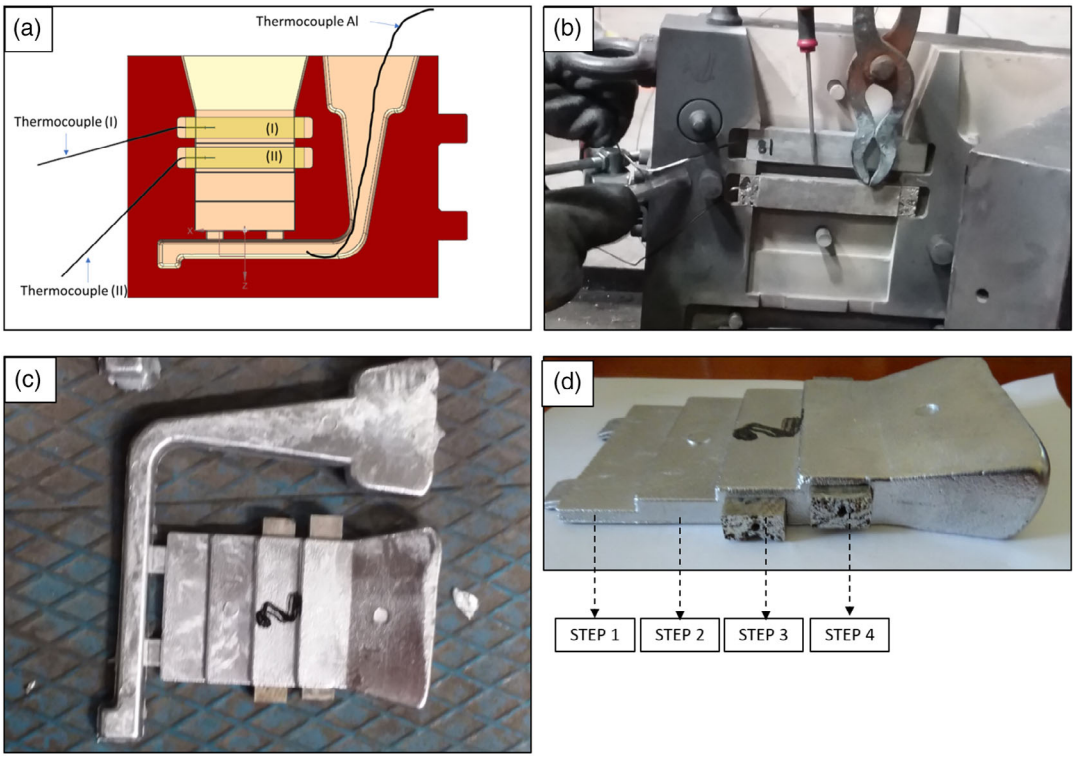


**Figure 2.** First set of experimental setups: a) scheme of the die, thermocouples, and foam cores positions, b) insertion of the foam cores, c) cast object produced, and d) transversal view of the stepped product obtained by casting with foam inserts (with an indication of the different steps).

the foam core placed in position (II) which, when the mold is closed, have a complete contact on one face with the movable wall of the mold. Therefore, the heating to the die temperature proceeds differently. During the liquid Al pouring, the foam in position (II) is lapped on 3 sides from the ascent of liquid aluminum, being the last side in contact with the moving part of the die, while in the case of the foam core in position (I), the heat exchange takes place on the 4 sides.

Furthermore, the recorded temperature measured in the foam core is influenced both by central thermocouple at its center, at a certain distance (minimum 5 mm) from the surface that comes into contact with the liquid, and by the thermal conductivity of the foam itself, resulting in a time delay in the recorded temperature increase, in the order of 12–17 s for the bottom core and of 15–21 s for the top core, for the six different samples.

### 2.3. Characterization

The chemical compositions of dense cast Al and Al foams were measured by means of OES, GNR—MetalLab32, after SiC abrasive paper grinding.

The density of the foam samples was experimentally verified by weight and volume measurements.

The co-fused samples (Figure 2d) were analyzed with the 160 KV—X-ray machine (Gilardini Company) or by means of CT (Tomograph Fhg, customized X-ray tomography system for nondestructive analyses) to investigate the inner core–shell interface and the porosity on the whole samples by nondestructive methods. In the case of CT scan analyses, the bonding between the foam core and the dense shell was investigated by VG Studio max software. After CT analyses, the samples were cut closer to the observed joining zones and analyzed metallographically. The CT-scan parameters used for the measurements are the following: 1) Acceleration voltage 200 kV. 2) Emission current 30 μA. 3) Projection number 800. 4) Integration time 1 s. 5) External filter Cu. 6) Voxel size 72.43 μm. 7) Focal spot size 3 μm.

Small samples of Al foams (not those inserted), the dense cast metal (from steps 1 and 2), and Al foams surrounded by cast metal (from steps 3 and 4) were transverse cut, mounted in resin and mirror polished for metallographic analyses.

The samples were observed by optical microscope (Reichert-Jung MeF3, Leica Microsystems Srl) and the images were processed by ImageJ software to determine the pore dimensions (the Feret's method, normally used for the measure of the sizes of irregular shape particles, was adopted for this purpose), the thickness of the skin and those of the pore walls of foam samples and the quality of the foam-dense metal interface in the cast objects.

The secondary dendrites arm spacing (SDAS) of cast Al samples (taken from steps 1 and 2) was estimated from 100× magnification optical images, by dividing the length of the principal dendrite by the number of secondary arms minus 1, as suggested in ref. [15]. SDAS can be correlated with metal cooling rate and with the final mechanical properties (e.g., microhardness) of the casting.[21–23]

The morphology and semiquantitative chemical composition of Al-foams surface and cross-section were investigated by means


© 2022 The Authors. Advanced Engineering Materials published by Wiley-VCH GmbH

of SEM-EDS JEOL, JCM 6000 plus and JED 2300. The quantification of elements with EDS has an error lower than 1% in the measurement conditions. The surface of Al foams were analyzed in the as-received conditions, after acetone washing (5 min in an ultrasonic bath), and after abrasive paper grinding and nitric acid etching to remove the surface scale followed by acetone washing. These surface preparations were aimed at the investigation of the surface composition and morphology (e.g., presence of surface contaminants and oxides, which can be progressively removed by washing and grinding) to better understand their influence on the interaction with the molten metal during the casting experiments. The resin-mounted foam samples were Cr sputter coated to facilitate SEM observations.

The average porosity was obtained from the density as $1-\rho_s$, where $\rho_s$ is the relative density, calculated as the foam density ($\rho$) divided by the aluminum density (2.7 g cm$^{-3}$).

The thermal conductivity was measured using the commercial instrument Hot Disk model TPS 500. The TPS 500 uses the transient plane source method[24,25] and is equipped with a sensor, a thin metallic double spiral positioned between two sheets made of Kapton, which functions as an electrical insulator. The sensor acts simultaneously as a heat source and a temperature detector. During the experiment, a stepwise current is applied to the sensor, which is positioned between the two samples of the material to be tested, causing a Joule heating and, consequently, a temperature transient in both sample and sensor. The analysis of this temperature transient allows determining the thermal conductivity of the specimens.

## 3. Results and Discussion

### 3.1. Characterization of the Foams

The chemical composition obtained from OES analyses is reported in **Table 1**. The Al foam contained Mg and Si as main alloying elements, with traces of other elements, as expected for the AlMgSi1 alloy.

**Table 1.** Chemical composition (wt%, average values of 4 measurements per sample type) of foams and cast metal from OES analyses.

| Element | Foam | Cast Al |
|---|---|---|
| | wt% | wt% |
| Si | 0.89 | 9.648 |
| Fe | 0.08 | 0.324 |
| Cu | 0.05 | 1.320 |
| Mn | 0.02 | 0.145 |
| Mg | 1.30 | 0.539 |
| Zn | 0.015 | 0.297 |
| Ni | 0.023 | 0.080 |
| Ti | >0.600[a)] | 0.060 |
| Sb | >0.100[a)] | 0.014 |
| Other | 0.018 | 0.055 |
| Al | rest | rest |

[a)]The symbol (>) indicates that the content of these elements is outside the range of the adopted standard for the chemical analysis.

A significant amount of Ti was detected in the chemical composition of the alloy. This is associated with the use of $TiH_2$ as a foaming agent, as reported in the Experimental Section.

The cast Al composition used is in line with the coded alloy (EN AB.46400).

The optical and electronic images of different foam cross sections are reported in **Figure 3** together with two representative EDS spectra.

The transverse section of the foam shows a thick skin, obtained by the production method and die shape, on all 4 sides of the bar profile from which the samples were taken (better defined hereafter), an extensive porosity, not homogeneously distributed, and characterized from thick cell walls, sometimes containing pores of smaller size. The morphology and the pores distribution in the foam are in accordance with the production method (powder metallurgy), which foresees the heating of metallic powders containing a small amount of foaming agent.

Furthermore, numerous polygonal-shaped particles, with dimensions of a few tens of micrometers, are visible on the cross-section of the foam in both optical and electronic images (red circles in Figure 3d–i). EDS analyses (Figure 3m) show that they are mainly made up of titanium with the presence of O, C, and Al. Titanium comes from the decomposition of the foaming agent ($TiH_2$) used in the production of the foam and its presence is in accordance with OES results (Table 1). In contrast, Ti was not detected on the metal matrix of the foam which shows a high percentage of Al (Figure 3l), confirming Ti's very low solubility in the matrix, while it is mainly concentrated in the particles themselves, together with some weight % of Al (near alpha alloy). EDS analyses conducted on the foam base material confirm the presence of Al and Mg (already detected by OES). The presence of Cr is ascribed to the sample Cr coating of resin-mounted samples for SEM observation.

The density of the three types of foams used as cores in the co-fusion tests was measured as the ratio of mass to volume in the available samples, obtaining the percentage of porosity as relative density with respect to the compact components with the same volume. However, since the distribution of porosity was not homogeneous (Figure 3a–c), partly due to the presence of the surface skin, the measurements of pore dimensions, wall and skin thicknesses on the metallographic transverse section of the used foam cores were conducted and the results are reported in **Table 2** and **Figure 4**.

The foam cores used in the present research in co-casting technology showed a density of 1.04, 1.28, and 1.53 g cm$^{-3}$ and relative calculated porosity of 60%, 50%, and 40% respectively.

Pores dimensions, wall, and skin thickness were evaluated by around or more than 100 measurements for each foam type and parameter performed on 10 digital images taken on the metallographic transverse sections and processed with the image analysis software (Image-J).

The greatest contribution to the differences in porosity of the Foams 1, 2, and 3 were the different wall thicknesses among the pores which progressively increased in average value and also, partly, in maximum thickness. A lesser contribution may be attributed to the different sizes of the pores which are however very


© 2022 The Authors. Advanced Engineering Materials published by Wiley-VCH GmbH

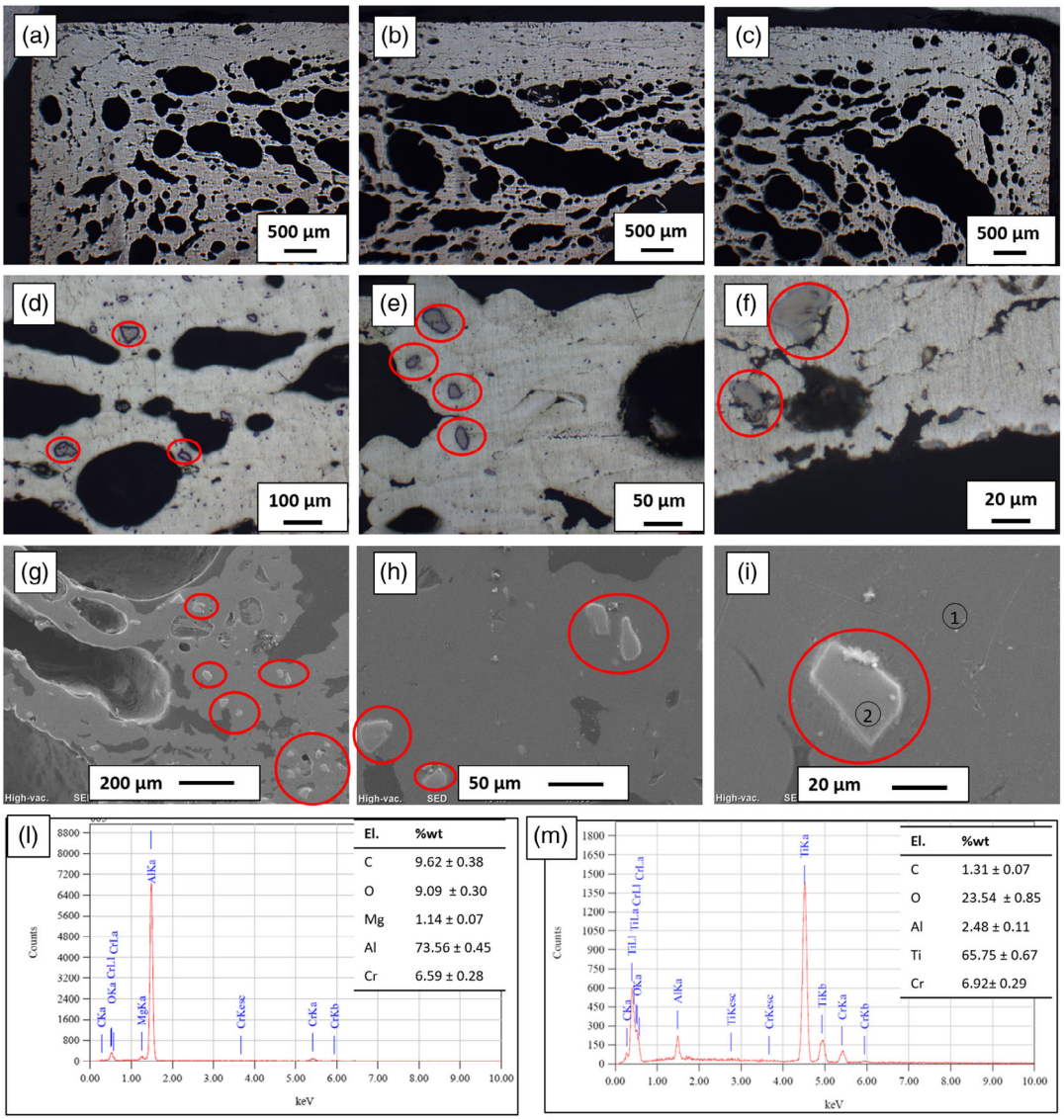


**Figure 3.** Optical microscopy images different areas of the same sample: a–c) at low and d–f) higher magnification, g–i) scanning electron microscope (SEM) images of cross-sections of foams used as inserts. Representative energy-dispersive spectroscopy (EDS) spectra of the foam: l) analysis related to area 1 in Figure 3i, and of a particle: m) analysis related to area 2 in Figure 3i). Red circles evidence the particles, observed by optical and electron microscopy, and analyzed by EDS.

similar (0.57–0.63 mm) for three Foams 1, 2, and 3, even taking into account the minimum and maximum pores sizes. Also, the thickness of the skin, which guaranteed a continuous surface layer, was between 0.1 and 0.4 mm and did not show a continuously increasing trend with the decrease in the amount of porosity.

The analytical results obtained from the pores sizes, the wall, and skin thicknesses show a considerable variability between the minimum and maximum values, confirming the inhomogeneity observed by metallographic analyses.

Considering the interface reactivity between the foam core and the liquid aluminum, one of the main issues which emerged from the analyses of cast objects with foam inserts without surface preparation (see Section 3.2 of the present article) was the complete absence of metallurgical bonding between the foam inserts and the cast metal. This phenomenon is often associated with an extremely low reactivity of the foam outer skin with the Al molten metal during casting, as widely reported in the literature.[5]

To better investigate this aspect, the surface morphology and chemical composition of the foam surfaces were analyzed by means of SEM and EDS. Three different surface preparations of the outer dense skin of the foams were considered: as received, washed, or ground and washed, as described in the Experimental Section. The main results are reported in **Figure 5**.

SEM images of the as-received (Figure 5b,c) and washed (Figure 5d,e) foams show the presence of a heterogeneous and porous surface scale.

The results of EDS analyses conducted on the surface dense skin of the foams (Figure 5a), highlight the presence of Al, O, C,


© 2022 The Authors. Advanced Engineering Materials published by Wiley-VCH GmbH

**Table 2.** Density (mean ± standard deviation), pore dimensions, pore wall thickness, skin thickness, and porosity of the used foams. Average values (obtained from around or more than 100 measurements for each foam type and parameters performed on 10 digital images of different transverse sections for each sample type).

| | Foam 1 | Foam 2 | Foam 3 |
|---|---|---|---|
| $\rho$ [g cm$^{-3}$] | 1.04 ± 0.007 | 1.28 ± 0.02 | 1.53 ± 0.02 |
| $\rho_s$ [relative density] | 0.40 | 0.50 | 0.60 |
| Mean Porosity (1−$\rho_s$) [%] | 60 | 50 | 40 |
| Pore dimension [μm] | | | |
| Mean | 566 | 568 | 635 |
| Min | 94 | 94 | 138 |
| Max | 2816 | 3934 | 3555 |
| Wall thickness [μm] | | | |
| Mean | 59 | 77 | 112 |
| Min | 15 | 13 | 24 |
| Max | 162 | 395 | 406 |
| Skin Thickness [μm] | | | |
| Mean | 122 | 447 | 321 |
| Min | 35 | 34 | 42 |
| Max | 313 | 1273 | 1204 |

and Mg as the main constituents, in accordance with the foam composition, while titanium was not detected on the surface. Even if EDS has a certain measurement error, more pronounced for low atomic weight elements such as carbon, some trends can be evidenced because the differences in the quantification of elements were always higher than 1%wt, which can be estimated as the measurement error. It can be observed that acetone washing reduced the carbon and oxygen content (attributable to carbon contaminants that comes from the die coating adopted in the production method to avoid surface adhesion between mold and sample) and made more evident the metallic Al and Mg constituents of the foam because acetone is not able to dissolve Mg-rich oxides. These oxides were mainly concentrated in numerous agglomerates on the surface, richer in magnesium. This result confirms the high tendency of Mg-containing Al alloys to form stable Mg-oxides on the surface.[26–28] The presence of Mg-carbonates can also be supposed due to the rather high carbon content. The permanence of Mg-rich oxides/carbonates after ultrasonic acetone washing suggests that they were firmly attached to the metal surface.

After surface grinding, the carbon and oxygen content, as well as the magnesium content decreased, suggesting that their concentration on the surface was higher than in the under layer and bulk metal.

For these reasons, surface grinding with SiC abrasive paper (320 grit) followed by nitric acid (12% Vol.) etching was applied on a set of foams to be used in a second casting experiment, as described in the Experimental Section.

The surface morphology and chemical composition of one sample of the second set of treated foams are reported in **Figure 6**. The foam surface appears whitened and opaque (Figure 6a). SEM observations show the typical appearance of grinded metallic materials with scratch tracks. The EDS analyses confirm the reduction of carbon, oxygen, and magnesium content with a higher aluminum percentage detected on the surface

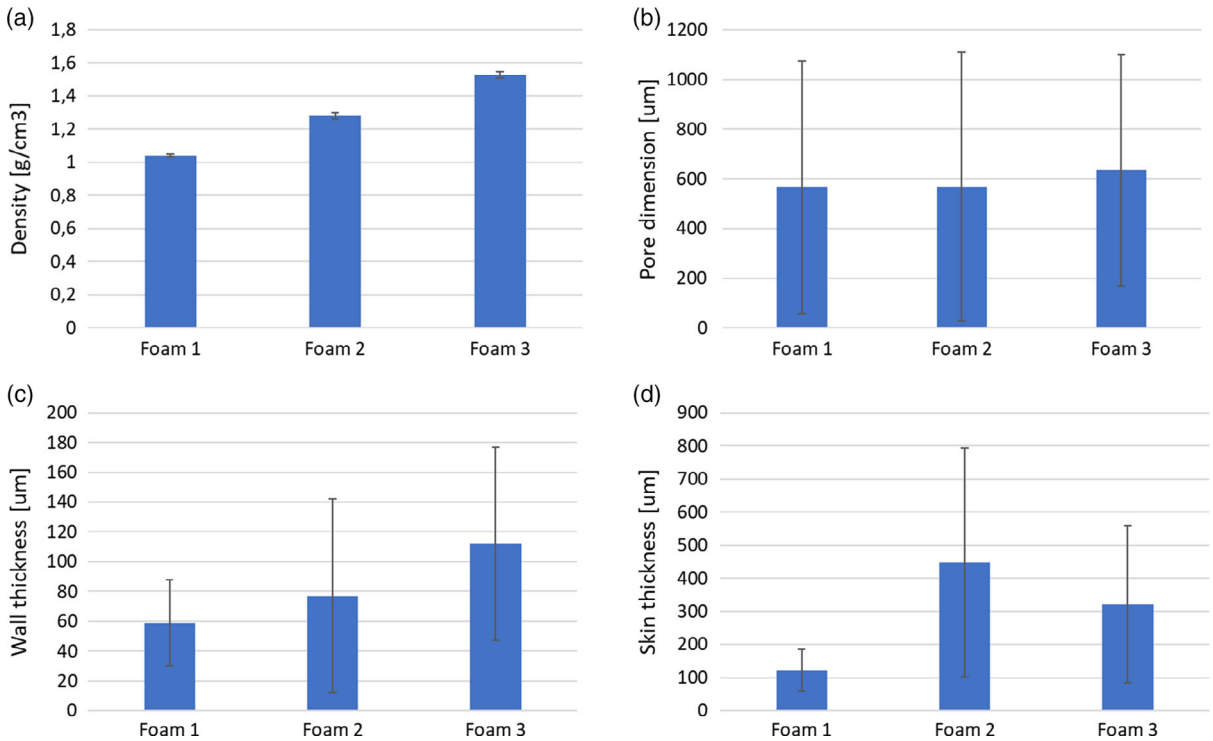


**Figure 4.** a) Bar diagram of density, b) pore dimension, c) wall thickness, and d) skin thickness for the various foams.


© 2022 The Authors. Advanced Engineering Materials published by Wiley-VCH GmbH

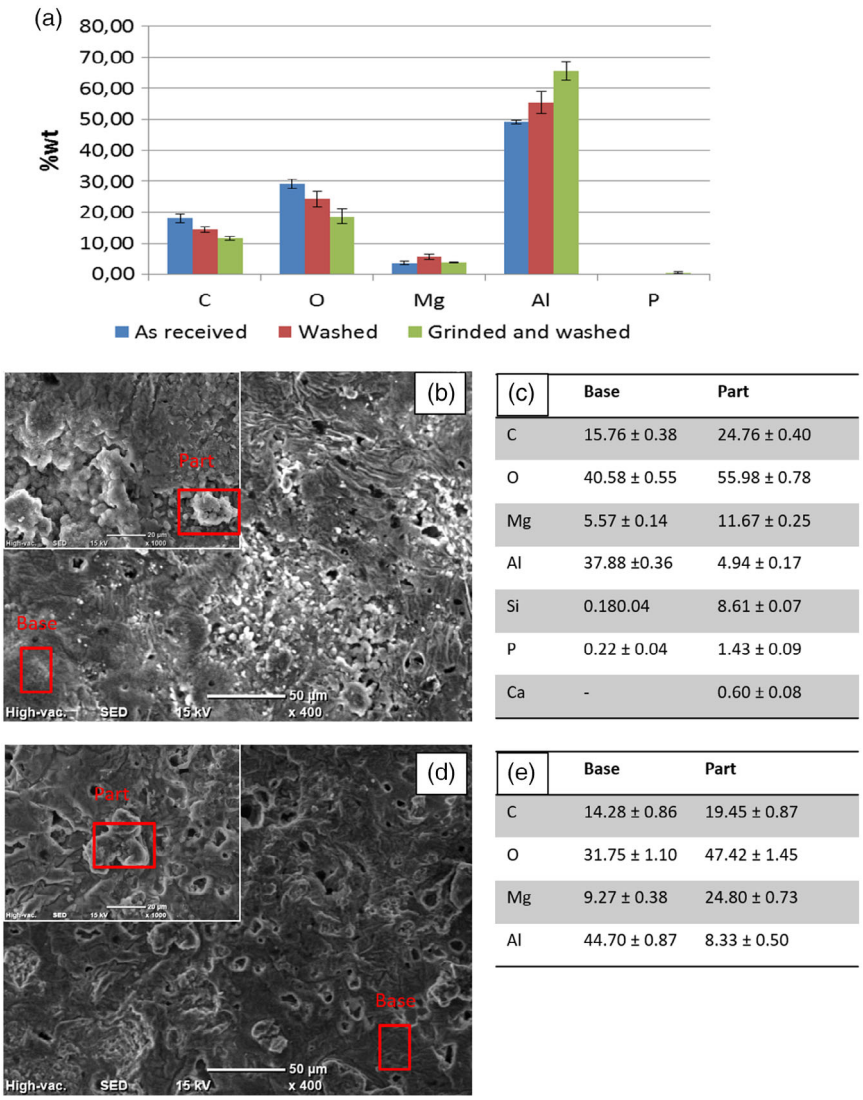


| (c) | Base | Part |
|---|---|---|
| C | 15.76 ± 0.38 | 24.76 ± 0.40 |
| O | 40.58 ± 0.55 | 55.98 ± 0.78 |
| Mg | 5.57 ± 0.14 | 11.67 ± 0.25 |
| Al | 37.88 ±0.36 | 4.94 ± 0.17 |
| Si | 0.180.04 | 8.61 ± 0.07 |
| P | 0.22 ± 0.04 | 1.43 ± 0.09 |
| Ca | - | 0.60 ± 0.08 |

| (e) | Base | Part |
|---|---|---|
| C | 14.28 ± 0.86 | 19.45 ± 0.87 |
| O | 31.75 ± 1.10 | 47.42 ± 1.45 |
| Mg | 9.27 ± 0.38 | 24.80 ± 0.73 |
| Al | 44.70 ± 0.87 | 8.33 ± 0.50 |

**Figure 5.** a) Graph reports EDS analyses of the foams outer skin as received and after some modes of surface preparation (washing, grinding, and washing) as mean and standard deviation of measurement performed on three different areas, b) SEM images of the as-received foam surface, c) EDS analyses on as received foam surface (wt% ± error rate), d) SEM images of washed foam surface, e) EDS analyses of washed foam surface. Red boxes represent the areas analyzed by EDS (wt% ± error rate).

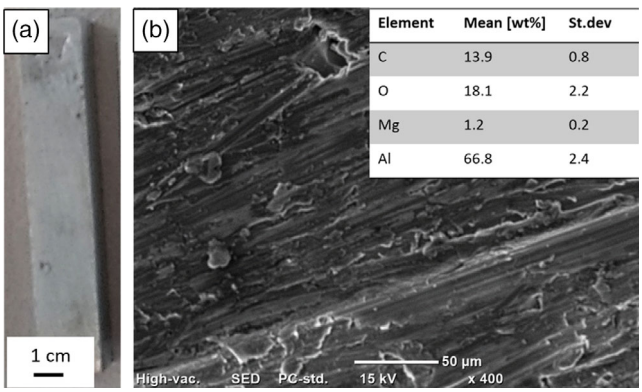


| Element | Mean [wt%] | St.dev |
|---|---|---|
| C | 13.9 | 0.8 |
| O | 18.1 | 2.2 |
| Mg | 1.2 | 0.2 |
| Al | 66.8 | 2.4 |

**Figure 6.** a) Macro image and b) SEM morphology and EDS analyses of the foam insert surface after surface grinding and $HNO_3$ etching.

when compared with surfaces that had not been grinded and etched.

The thermal conductivity properties were measured with the instrument TST 500, which gives material values in the range $0.03 \div 100\,\mathrm{W\,m^{-1}\,K^{-1}}$, with an accuracy of ±5%, however outside the values expected for both specimens of dense Al casting and ones of Foams 1, 2, and 3.

A set of foam samples from the same family as those in the present work was therefore used, but with a relative density of 0.13 and 0.15, a thickness of 11 mm, and the sides of about $100 \times 100$ mm. Due to the high porosity of these specimens, the instrument was equipped with the largest available sensor (6.403 mm in radius), to perform the measurements on a representative area of the sample. The measurements, carried out at room temperature, were repeated several times by positioning


© 2022 The Authors. Advanced Engineering Materials published by Wiley-VCH GmbH

the sensor in different areas on the sample surface. The average thermal conductivity obtained was 8.8 $W\,m^{-1}\,K^{-1}$.

Furthermore, Equation (1), reported in the literature, was used to scale the thermal conductivity value of dense Al/Al-alloys ($\lambda_{Al}$) to the one of metal foams ($\lambda_F$)[2]

$$\lambda_F = \lambda_{Al}(\rho_F/\rho_{Al})^q \tag{1}$$

with the exponent q in the range 1.65–1.8.

The measured thermal conductivity (8.8 $W\,m^{-1}\,K^{-1}$) is in accordance with the ones reported in the literature for closed cells aluminum foams with a dense outer skin[1] as well as with the values obtainable using Equation (1) for aluminum foams with the tested reduced density (6–9 $W\,m^{-1}\,K^{-1}$), considering the thermal conductivity of AlMgSi alloy as 218 $W\,m^{-1}\,K^{-1}$.[29]

Therefore, the adopted Equation (1) is certainly usable to calculate the thermal conductivity of Foams 1, 2, and 3[24,30] and the obtained values of thermal conductivity in the ranges 36–42 $W\,m^{-1}\,K^{-1}$ for Foam 1, 58–65 $W\,m^{-1}\,K^{-1}$ for Foam 2, and 76–83 $W\,m^{-1}\,K^{-1}$ for Foam 3, used in the present research.

These experimental observations can be useful for a better interpretation of the thermal behavior of foam inserts in casting experiments.

### 3.2. Characterization of Cast Objects

Optical microscope images and SEM-EDS analyses of dense cast aluminum (Steps 1 and 2 of the cast object) are reported in **Figure 7**. The microstructures show the typical dendritic morphology of cast Al alloys, in which the lighter grains are the aluminum-rich α phase and the darker zones (interdendrites) refer to the Al–Si eutectic microstructure (well visible in the 500× images, Figure 7c,d). Numerous gray particles, with irregular shape (red circles in Figure 7c,d) can be observed at 500 magnifications; EDS analyses conducted on structures with the same morphology and dimensions (Figure 7e,f) show the presence of a significant amount of Fe and Cu, which suggests

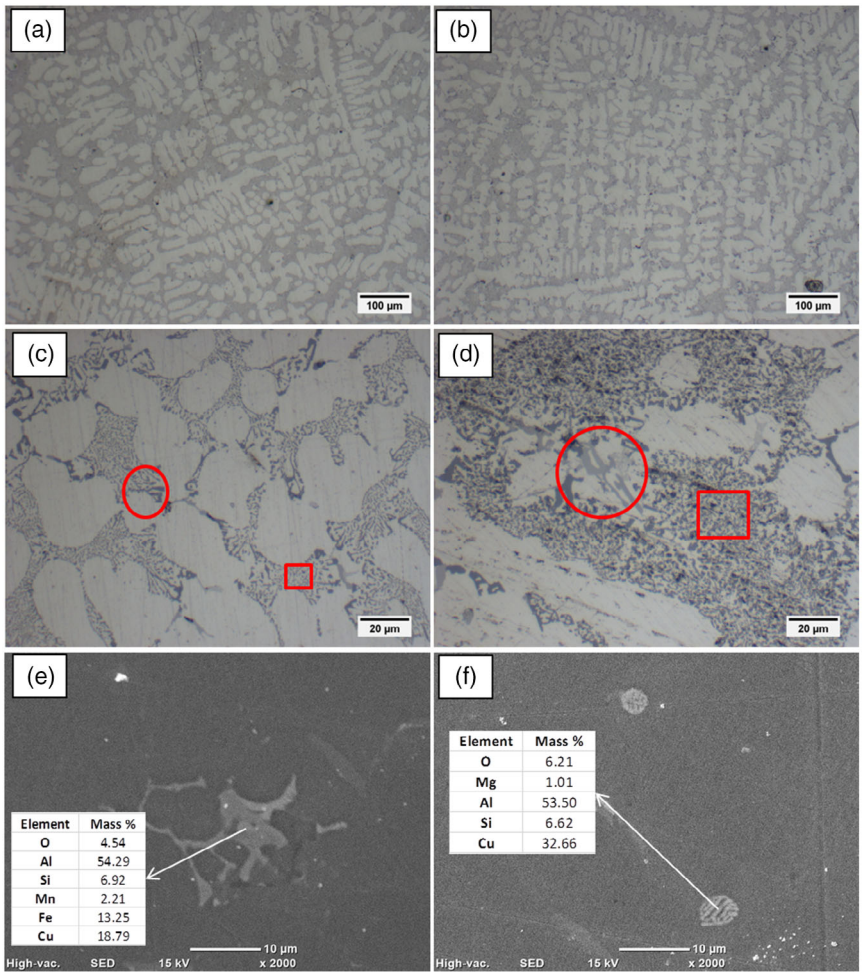


**Figure 7.** a) Optical microscopy (OM) image (100×) of cast Al-step 1, b) OM image (10×) of cast Al-step 2, c) OM image (500×) of cast Al-step 1, d) OM image (500×) of cast Al-step 2, e) SEM image with EDS analysis of the detail, of cast Al-step 1, f) SEM image with EDS analysis of the detail, of cast Al-step 2. Red circles/boxes highlight second phases particles analyzed by EDS.


© 2022 The Authors. Advanced Engineering Materials published by Wiley-VCH GmbH

the possible formation of second phases such as $Cu_2FeAl_7$ or $(Fe, Mn)_3SiAl_{12}$.

The SDAS measurements evidenced an average value of $17.7 \pm 2.9$ µm for step 1 and $20.2 \pm 4.5$ µm for step 2 of the die. The difference is limited but it is in accordance with the higher cooling rate where the die is thinner—step 1, which can lead to a smaller SDAS value, as reported in the literature.[21–23]

**Figure 8** reports the temperature versus time trend for the aluminum, the die, and the two foam inserts for the first experiment (Figure 8a), the temperature rise for two foam inserts, with different densities, in position (I), always in the first experiment (Figure 8b) and the curves graphs of temperature versus time, for the foam inserts in position (I) in the first (without surface treatment) and in the second (with surface grinding and etching) experiments (Figure 8c).

In the first experiment, during the Al casting, the thermocouple that measures the temperature of the liquid in the cavity shows a sudden increase in around 2–3 s, it reaches a maximum (from 643 to 682 °C for the different samples) and, after a sudden decrease in 4 s, shows a sort of slow cooling in the temperature range from 575 to 520 °C when the liquid–solid coexistence and miscibility gap occur, and then the slope highlights another increase of cooling rate going towards the die temperature.

During the pouring of the die, the foam specimens in position (II) reach their highest temperatures (comprised between 460 and 520 °C) in a shorter time than those in position (I) because they are the first cores to be reached from the flowing liquid.

However, the highest temperatures are reached from the top inserts, position (I), because the liquid Al flows touching the four heat exchange surfaces of the cores, which are even closer to a greater thermal mass of liquid (on the top); the bottom core, in position (II), is instead in contact with the liquid Al with three heat exchange surfaces, being the fourth in contact with the moving die surface, which has a lower temperature than the liquid metal and exchange heat with the insert. It should furtherly be noted that the maximum temperature recorded by the thermocouple, located at the center of the foam inserts, is only a few degrees higher than the minimum existence temperature of the liquid, which remains in contact with the foam surface for only a few seconds and then the aluminum starts solidification from around 564 °C, considering the Al–Si phase diagram, the composition of the alloy and the slope trend of the cooling curve. In fact, the red curve of Figure 8a shows, after a rapid increase in temperature, an equally rapid decrease, and an evident change in slope at this temperature, evidencing the start of the formation of the solid. Together with the demonstrated low surface reactivity of foams due to the presence of Mg in the form of oxide, the reduced time of contact between liquid aluminum and solid foam justifies the observed absence of chemical bonding.

Finally, by comparing the decrease in the temperature of both the inserts (top and bottom) has to be observed that the foam insert in the top position (I) always cools more slowly than the lower one and this is associated with the higher amount of thermal mass in the sprue placed above.

The comparison of rise of temperature of the foam inserts, in case of different densities, in position (I) in the first experiment is shown in Figure 8b. By the slope of the linear tract, the heating rate can be calculated and values of about 28 and 38 °C $s^{-1}$ can be obtained for insert with minimum (1 g $cm^{-3}$) and maximum

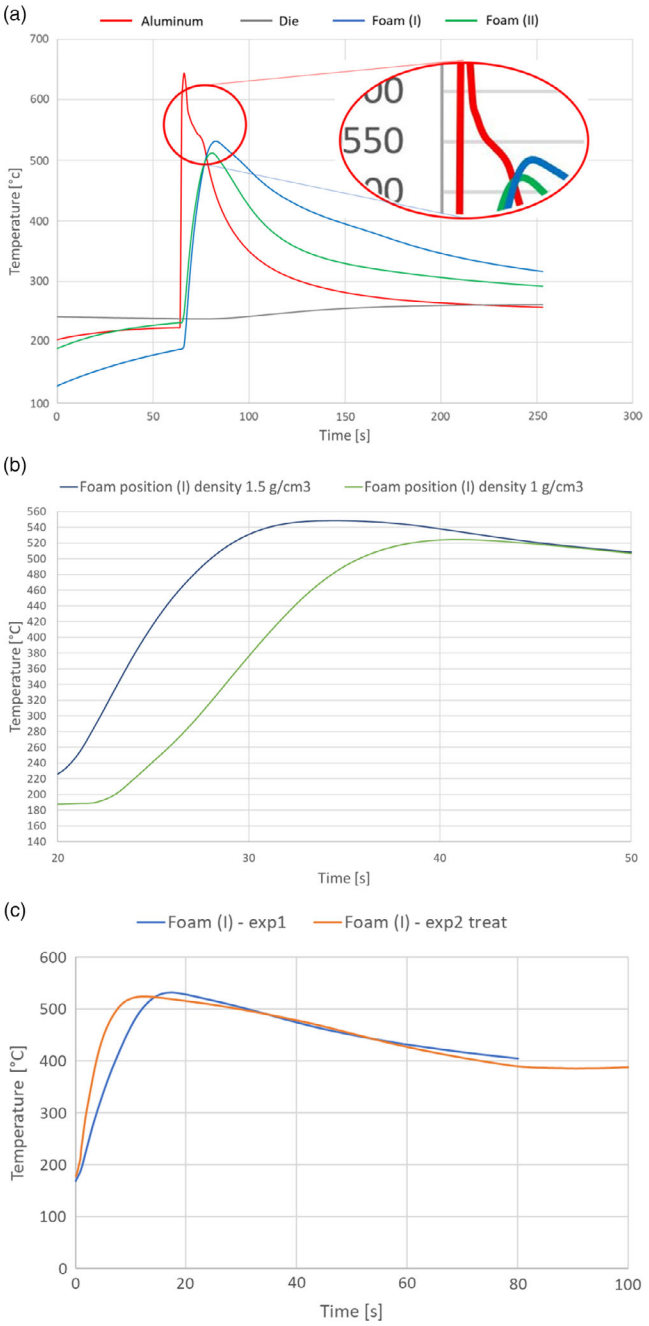


**Figure 8.** a) Temperature versus time for aluminum, die, and foam inserts in the first experiment; b) comparison of the temperature rise ramps for foam inserts in position (I) with different densities in the first experiment, c) example of temperature trend versus time for foam inserts of the first experiment (untreated) and of the second one (treated).

(1.5 g $cm^{-3}$) densities respectively. In accordance with the measured and calculated values of thermal conductivity of the foams in the function of density, the foam with higher density presents a more rapid temperature increase.

The comparison between the temperature increase in the Foam inserts in position I for the two surface treatments (and experiments) (Figure 8c) evidence that in the second experiment


© 2022 The Authors. Advanced Engineering Materials published by Wiley-VCH GmbH

the temperature rise is slightly more rapid than in the first experiment. This result can mainly be attributed to the surface removal of the surface oxides and carbonates (which are modest thermal conductors) increasing the heat exchange coefficient of the foam, while the maximum temperature of the inserts in position I is around the same.

Moreover, the time at temperatures above 500 °C was quite long in the second experiment, allowing a longer contact time between liquid aluminum and foam surface. This time can be further improved by means of core and die pre-heating.

The confirmation of the limited contact time between the liquid aluminum and the foam surface in the first experiment may be observed on the metallographic cross-section of the cast component in position (II), **Figure 9**, where the liquid aluminum was in contact with the die on one side and with the foam core on the other.

In particular, the observation of the microstructures of Figure 9a,c shows dendritic morphologies that progressively increase in arm sizes, both in length and in diameter, moving from surface to a depth of more than one millimeter toward the center, on both sides.

The images taken at higher magnification, shown in Figure 9b,d, of the surface microstructure of the solidified aluminum in contact with the die and the foam core, respectively, reveal a refined dendritic microstructure, slightly less defined in the dendrite arms on the foam side.

Basically, at the center of the Al cast part, in correspondence with insert II, it can be observed the same morphologies shown in Figure 7c,d observed at the center of the dense cast metal, without foam (in step 1). The comparison between the microstructure of Figure 9b–d, at the surface, and those of Figure 7c,d, at the core, better evidence that the surfaces have a finer dimension of the dendrite arms, with also a lower presence of regular and ordered arms, as well as a smaller dimension of the second phase particles in the interdendritic areas.

The phenomenon was still more evident in the microstructure of the surface in contact with the foam, probably because of the direct contact of the liquid with the surface of the metallic foam itself, while the inner surface of the die was coated with an anti-adhesive ceramic coating, which slightly decreases the surface heat exchange coefficient. In contrast, the foam presents a thick surface skin (of dense Al-alloy) with the substantially higher thermal conductivity of the compact. The data on thermal conductivity of the foams, previously reported in this article, from measurements and calculations, supported this hypothesis. In fact, the core foams present a thermal conductivity ranging between 20% and 40% of the one of dense aluminum and the dense skin has a thermal conductivity reasonably close to the bulk metal one.

These observations supported the hypothesis of a faster cooling rate of the liquid aluminum and the quick formation of a solid skin upon contact with the foam, with a consequent short contact time between liquid metal and the foam surface which did not favor reactions and metallurgical bonding, in the first experiment.

The visual appearance of the region of foam inserts in the cast objects from the first experiment, Figure 9 (metallographic sample on the left) and 10a, shows that no infiltration of the foams occurred due to the presence of a thick dense external skin

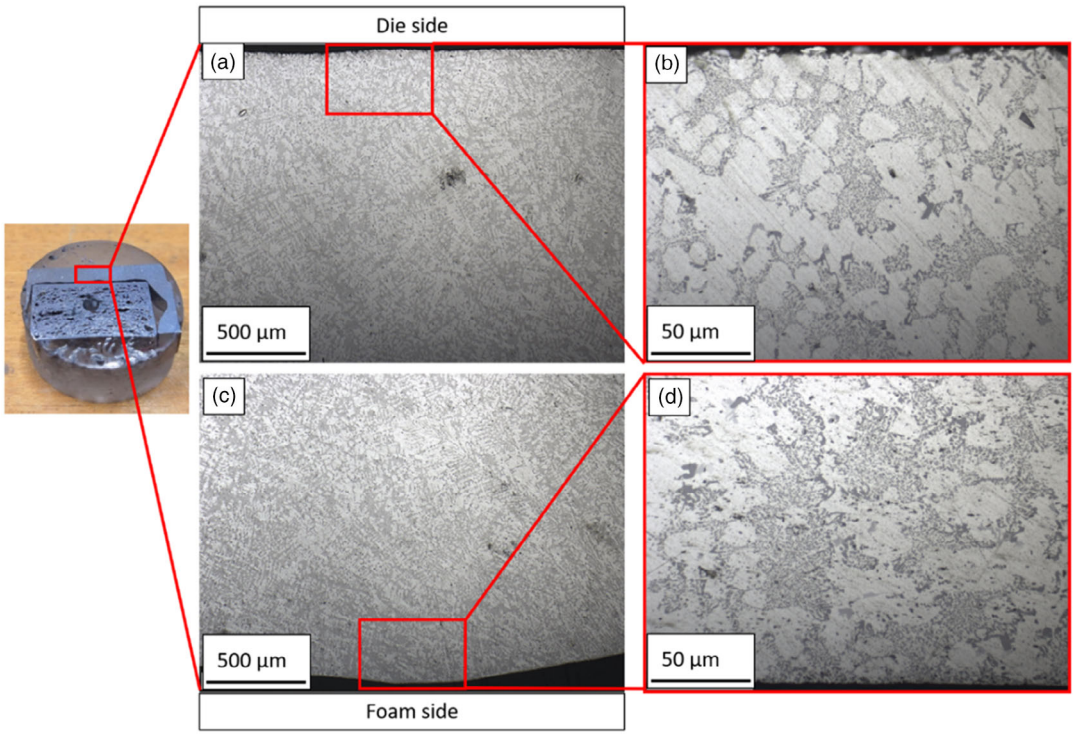


**Figure 9.** Metallographic sample from the cast specimen (on the left). OM of the cast metal around the foam core: a,b) optical images at 50× and 500×, respectively, of the cast metal from the die side; c,d) optical images at 50× and 500×, respectively, of the cast metal from the foam side.


© 2022 The Authors. Advanced Engineering Materials published by Wiley-VCH GmbH

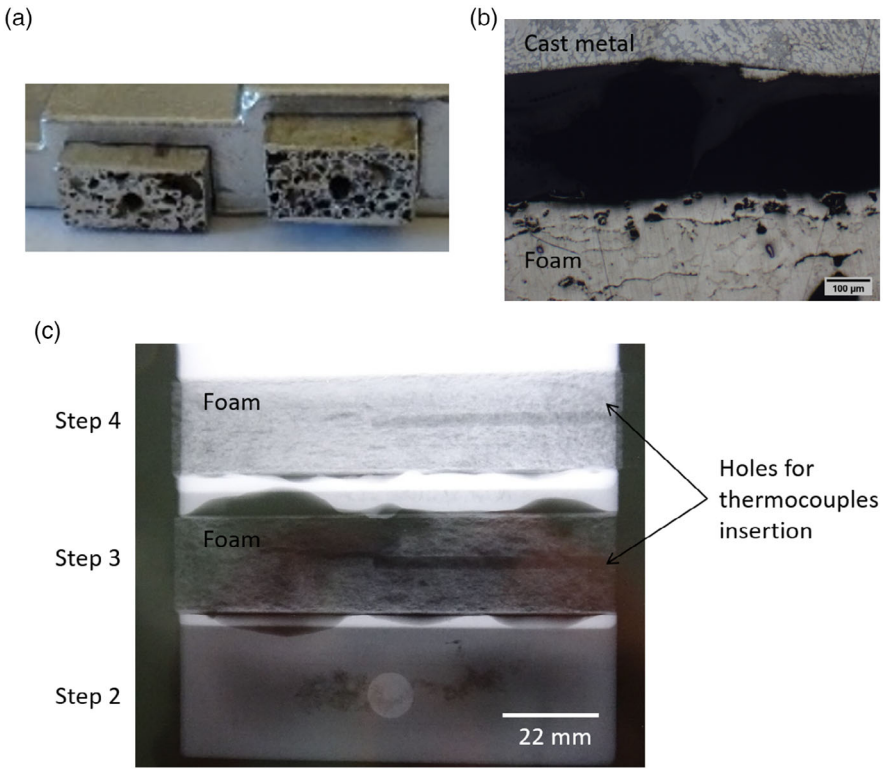


**Figure 10.** Visual, optical, and radiographical analyses of cast objects from the first experiment, a) photograph of a detail of a cast component with two foam cores, b) optical microscope image of the foam-dense metal interface in a sample of cast object, c) X-ray image of a cast object with foam inserts placed in positions I and II (steps 3 and 4, respectively).

of foam inserts, allowing the maintenance of foam inserts shape and porosity.

The presence of a gap (of about 200 µm) at the interface between the foam core and the dense metal in cast objects is also shown in **Figure 10**b. This gap indicates that no bonding between the two parts occurred and the poured Al during solidification and cooling has shrunk. The X-ray image of one of the cast objects shows the transverse thickness and density of the co-cast component in steps 2, 3, and 4 of the step-die, Figure 10c: the darker areas correspond to zones with a lower amount of material, (e.g., cavities, porosity, etc.) while the brighter ones are associated with higher amount of material, that adsorb more the transmitted X-rays. In the figure, the foam inserted in step 4 appears lighter than the one in step 3 because it is surrounded by a higher thickness of dense metal while the foam insert in step 3 has a "free face," as described in the Experimental Section. The dark areas around the foam insert in step 3 can be ascribed to not good die filling and shrinkage cavity due to the rapid solidification and contraction of the molten metal after the contact with the foam insert. Moreover, a dark line can be observed around both foam inserts and can be associated with the absence of bonding between the foam and the dense metal, as confirmed by OM (Figure 10b). The darker lines observable at the center of the inserts are the drilled holes produced for thermocouples insertion.

The macro image, OM analyses, and CT images of a cast object with a foam insert surface abraded and etched—second experiment—are reported in **Figure 11**. In this case, the photo image of the rough-cut surface shows an apparent continuity in many parts of the interface and some evident gap, caused by solidification shrinkage, in other parts. The metallurgical continuity can be observed also both on the optical images (Figure 11b,c) and on CT images (Figure 11d). The metallographic section of Figure 11c has been prepared by cutting the cast object in one of the zones of bonding evidenced by CT-scan analyses to better investigate surface reactions and joining. CT scan allows to analyze the whole sample in a non-destructive way and, in this particular case, it allows to investigate the extent of core–shell bonding across the entire interface evidencing several joined areas, which can be localized and observed at the optical microscope (after proper preparation of the selected section). In particular, in Figure 11c, it is observable a metallographic continuity between the Al-foam side and the cast metal that produce mainly an interdendritic microstructure.

The difficulty in the bonding between foams cores and dense shells has been reported in the literature for co-casting of Al and Al foams.[6,7,9] This bonding difficulty is attributed to the presence of aluminum and/or magnesium oxides (inert and with higher melting temperature) on the foam surface which can hamper the reaction between the foam skin and the melt metal.

These findings were confirmed by the first casting experiment reported in the present article, in fact, no bonding between the foam core and cast metal shell was observed with untreated foam


© 2022 The Authors. Advanced Engineering Materials published by Wiley-VCH GmbH

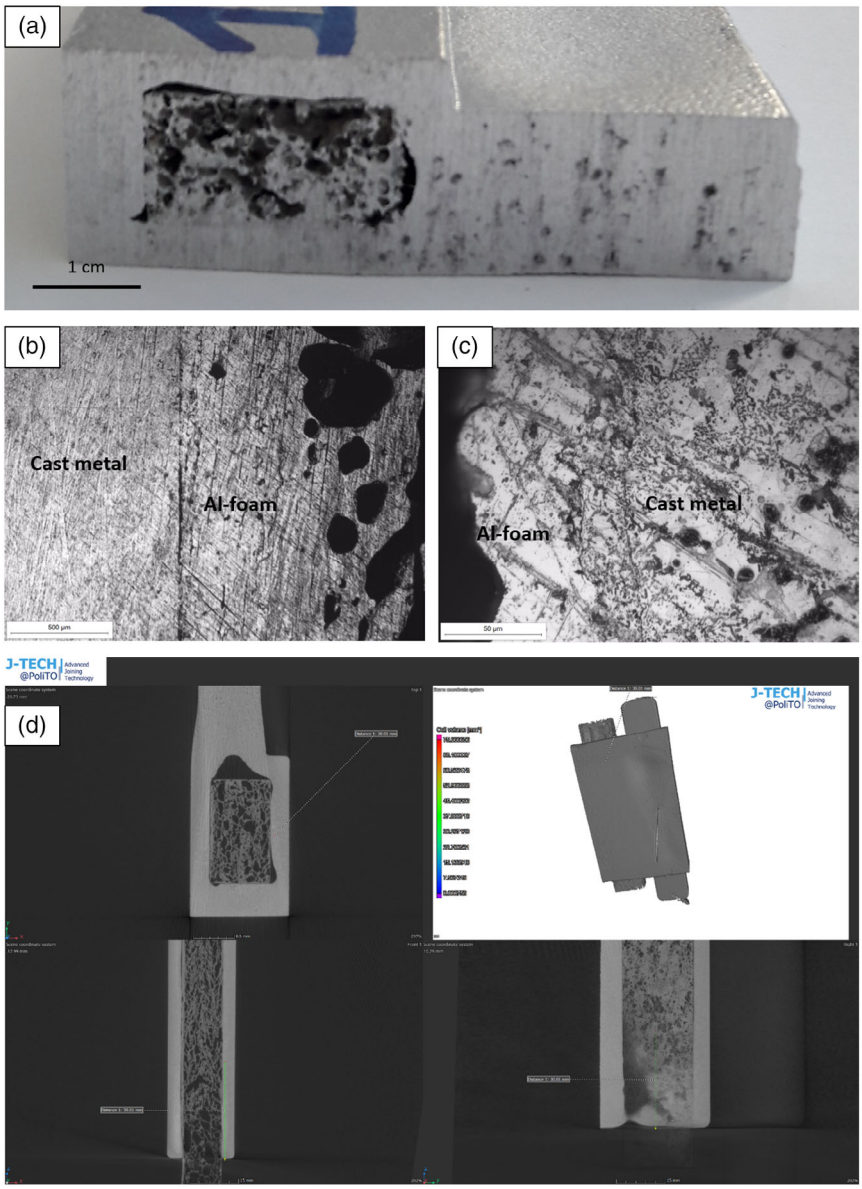


**Figure 11.** Visual, optical, and computed tomography (CT) analyses of cast objects from the second experiment, a) Macro image, b,c) OM images of the interface line between the foam core and the cast shell, d) CT images of a cast specimen with surface treated foam insert.

cores characterized by the presence of a high amount of magnesium oxides and carbonates on their surface. The grinding and etching preparation, with the consequent removal of surface oxide and carbonates, enhance the reactivity of the surface skin of the foam with the liquid metal as evidenced in the second casting experiment. According to these results, co-casting experiments by the authors, using foam cores with thin outer skin almost free from stable surface oxides, reveal a good bonding.[31] However, the absence of a thick skin did not prevent infiltration in this case.

This surface treatment is a fast, not expensive, and automatable process that can be promisingly adopted for the improvement of the industrial application of this technology.

The partial melting of the foam skin has been reported as a successful strategy for the obtainment of a core–shell metallurgical bonding.[8,10,18,32] From this standpoint, the time at melting temperature of the foam surface has been shown to be too short and not sufficient to induce the surface foam melting in the first experiment. In the second experiment, the situation was instead improved also from this standpoint, however, the surface melting of the foam cores did not occur on the whole insert surface. Core and die pre-heating can be considered to further improve the process setup.

It must be underlined that the presence of a mechanical and metallurgical continuity between the foam core and the cast shell can be of interest to obtain enhanced mechanical properties;


© 2022 The Authors. Advanced Engineering Materials published by Wiley-VCH GmbH

however, the presence of some discontinuities can be useful for damping properties.[14]

## 4. Conclusion

The present research reports a detailed study on the possibility to use Al-based foams as permanent cores in Al-based cast objects. Al-foams with different densities (1, 1.3, and 1.5 g cm$^{-3}$) and with a dense outer skin were characterized and used as inserts in Al casting experiments.

The presence of a thick (150–450 μm) and continuous dense skin successfully preserved foam inserts from infiltration of the molten aluminum, thus maintaining the initial porosity. In contrast, without foam surface preparation, no bonding between the foam core and the cast shell was obtained. The presence of aluminum oxide on the surface of the foam skin and the short contact time between liquid aluminum and the foam surface during casting have been reported in the literature as possible causes of this phenomenon. Interestingly, the absence of core–shell joining can even be advantageous if the main aim of the final cast object is an improvement of damping properties.

Foam surface grinding and etching were tested as a possible low-cost surface treatment for the removal of inert magnesium oxides and carbonates. In this second case, metallurgical bonding was obtained on several areas of the interface between the foam core and the cast metal shell. The presence of a stable bonding was useful for the improvement of the mechanical properties of the cast object.

This study highlighted that foam cores with a thick outer skin and a proper surface preparation can be successfully used as permanent cores in casting with sustainable production costs.

The main advantages of this application were weight reduction, energy/vibration absorption, and no need for core removal.

## Acknowledgements

DACA-I and Regione Piemonte are kindly acknowledged for funding this activity through ICARO project (ICARO- Industrialization of Cast Aluminum pROduct, call "Competitività regionale e occupazione" F.E.S.R. 2014/2020 Obiettivo tematico OT 1—Asse I—Azione I.1b.1.1 "IR2").

Open Access Funding provided by Politecnico di Torino within the CRUI-CARE Agreement.

## Conflict of Interest

The authors declare no conflict of interest.

## Data Availability Statement

Research data are not shared.

## Keywords

aluminum, casting, foam cores, metal foams

Received: January 21, 2022
Revised: February 23, 2022
Published online:

[1] H. P. Degischer, B. Kriszt, *Handbook of Cellular Metals: Production Processing and Applications*, Wiley-WHC, Weinheim, Germany, **2002**.
[2] M. F. Ashby, A. G. Evans, N. A. Fleck, L. J. Gibson, J. W. Hutchinson, H. N. G. Wadley, *Metal Foams: A Design Guide*, Butterworth-Heinemann, Oxford, UK **2000**.
[3] J. Banhart, *MRS Bull.* **2003**, *28*, 290.
[4] C. Korner, R. F. Singer, *Adv Eng Mat* **2000**, *2*, 159.
[5] G. Ubertalli, S. Ferraris, *Metals* **2020**, *10*, 1592.
[6] B. Bauer, S. Kralj, M. Busic, *Tehnicki vjesnik* **2013**, *20*, 1095.
[7] F. Simancik, F. Schoerghuber, *Mater. Res. Soc. Symp. Proc.* **1998**, *521*, 151.
[8] C. Cingi, E. Niini, J. Orkas, *Colloid Surf A* **2009**, *344*, 113.
[9] I. Vicario, I. Crespo, L. M. Plaza, P. Caballero, I. K. Idoiaga, *Metals* **2016**, *6*, 24.
[10] J. Babcsan, S. Essel, N. Karni, G. Szamel, S. Beke, N. Babcsan, *Resolut. Discovery* **2017**, *2*, 1.
[11] W. Dai, S. Xue, J. Lou, Y. Lou, S. Wang, *Trans. Nonferrous Met. Soc. China* **2012**, *22*, 30.
[12] S. P. Hu, C. N. Niu, H. Bian, X. G. Song, J. Cao, D. Y. Tang, *Mater. Lett.* **2018**, *218*, 86.
[13] D. Wei, X. Songbai, S. Bo, L. Jiang, W. Suiqing, *Rare Metal Mater. Eng.* **2013**, *42*, 2442.
[14] S. Ferraris, S. Perero, G. Ubertalli, *Coatings* **2019**, *9*, 459.
[15] G. Ubertalli, M. Ferraris, M. K. Bangash, *Compos. Part A* **2017**, *96*, 122.
[16] C. Korner, M. Hirschmann, H. Wiehler, *Mater. Trans.* **2006**, *47*, 2188.
[17] R. F. Singer, F. Heinrich, C. Korner, G. Grotzschel, Patent U. S. 6675864B2, **2004**.
[18] W. Knott, B. Niedermann, M. Recksik, A. Weier, Patent U. S. 6854506B2, **2005**.
[19] W. Knott, B. Niedermann, M. Recksik, A. Weier, Patent U. S. 6874562 B2, **2005**.
[20] F. Dobesberger, H. Flankl, D. Leitlmeier, A. Birgmann, Patent U. S. 2006/0029826 A1, **2006**.
[21] E. Hajjari, M. Divandari, *Mater. Des.* **2008**, *29*, 1685.
[22] L. Y. Zhang, Y. H. Jiang, Z. Ma, S. F. Shan, Y. Z. Ji, C. Z. Fan, W. K. Wang, *J. Mater. Process. Technol.* **2008**, *207*, 107.
[23] Y. Birol, *Mat Sci Eng A* **2013**, *559*, 394.
[24] M. A. Rodríguez-Pérez, J. A. Reglero, D. Lehmhus, M. Wichmann, J. A. de Saja, A. Fernández, in *Proc. of HT2009, 2009 ASME Summer Heat Transfer Conf.*, San Francisco, CA, USA, July 19–23 **2009**.
[25] E. Solórzano, J. A. Reglero, M. A. Rodríguez-Pérez., D. Lehmhus, M. Wichmann, J. A. de Saja, *Int. J. Heat Mass Transfer* **2008**, *51*, 6259.
[26] D. Wei, X. Songbai, S. Bo, L. Jiang, W. Suiqing, *Rare Met. Mater. Eng.*, **2013**, *42*, 2442.
[27] B. Xiao, D. Wang, F. Cheng, Y. Wang, *Appl. Surf. Sci.* **2015**, *337*, 208.
[28] Z. Zhu, Y. Chen, A. A. Luo, L. Liu, *Scr. Mater.* **2017**, *138*, 12.
[29] ASM International, *A. S. M. Handbook, vol. 2: Properties and Selection: Nonferrous Alloys and Special-Purpose Materials*, ASM International, Materials Park, OH **1990**.
[30] G.-Y. Lu, B.-Y. Su, Z.-Q. Li, Z.-H. Wang, W.-D. Song, H.-P. Tang, *Therm. Sci.* **2014**, *18*, 1619.
[31] S. Ferraris, A. Santostefano, A. Barbato, R. Molina, G. Ubertalli, *Metals* **2021**, *11*, 1715.
[32] C. Domrong, S. Srimanosaowapack, *J. Chem. Eng. Mater. Sci.* **2017**,*8*, 37.


© 2022 The Authors. Advanced Engineering Materials published by Wiley-VCH GmbH